

Approximation of Mie scattering parameters in near-infrared tomography of normal breast tissue *in vivo*

Xin Wang

Dartmouth College
Department of Physics and Astronomy
Hanover, New Hampshire 03755

Brian W. Pogue

Shudong Jiang

Xiaomei Song

Keith D. Paulsen

Dartmouth College
Thayer School of Engineering
Hanover, New Hampshire 03755

Christine Kogel

Steven P. Poplack

Dartmouth Medical School
Department of Diagnostic Radiology
Hanover, New Hampshire 03755

Wendy A. Wells

Dartmouth Medical School
Department of Pathology
Hanover, New Hampshire 03755

Abstract. A method for estimating Mie theory scattering parameters from diffuse light tomography measurements in breast tissue is discussed. The approach provides an estimate of the mean particle size and number density given assumptions about the index of refraction change expected in lipid-membrane-bound scatterers. When using a sparse number of wavelengths in the reduced scattering spectra, the parameter extraction technique is limited to representing a continuous distribution of scatterer sizes that appears to be dominated by an exponential decrease with increasing particle size. The fitting method is tested on simulated data and then on Intralipid-based tissue-phantom data, giving a mean particle size of 93 ± 17 nm, which is in excellent agreement with expectations. The approach is also applied retrospectively to breast tissue spectra acquired from normal healthy volunteers, where the average particle size and number density were found to be in the range of 20 to 1400 nm. Grouping of the data based on radiographic breast density, as a surrogate measure of tissue composition yielded values of 20 to 65, 25 to 200, 140 to 1200, and 150 to 1400 nm, respectively, for the four BI-RADS (American College of Radiology Breast Imaging Reporting and Data System) density classifications of extremely dense, heterogeneously dense, scattered, and fatty. These results are consistent with the microscopic characteristics of each breast type given the expected progression from predominantly collagenous connective tissue (extremely dense category) to increasing proportions of glandular epithelium and fat (intermediate density categories) to predominantly fat (fatty category). © 2005 Society of Photo-Optical Instrumentation Engineers. [DOI: 10.1117/1.2098607]

Keywords: particle sizing; Mie theory; infrared; tomography; tissues.

Paper SS04238R received Dec. 3, 2004; revised manuscript received Jan. 11, 2005; accepted for publication Jan. 18, 2005; published online Oct. 10, 2005.

1 Introduction

Near-infrared (NIR) tomography uses measured light propagation through tissue to generate images of internal distributions of optical absorption and scattering at multiple wavelengths. Over the past decade, there has been considerable interest in developing the approach as a breast-imaging modality to characterize abnormalities noninvasively.¹⁻⁷ Recent studies have shown that there is excellent contrast in breast lesions relative to normal tissue, and that the scattering contrast between malignant and benign processes appears to be significant.⁸ At the same time there have been important advances in particle sizing through Mie scattering theory,⁹⁻¹⁸ which is the model of light scattering that is applicable when the scatterer particle size is near the same dimension as the wavelength of radiation being scattered. Further, interest exists in exploiting the scattering spectrum of tissue to charac-

terize its microscopic properties, which may provide fundamental insight into the morphological features that are observed in the macroscopic diffuse light signal.^{9-13,19,20} In this paper, a method is presented to analyze bulk-tissue-reduced scattering spectra in terms of their approximate Mie scatterer parameters.

When exploring a method to characterize scatter size and density, it is important to focus on what is known and not known about how light scatters in tissues consisting of normal and malignant cells. The morphologic changes from normal to diseased breast tissue are seen by light microscopy in the cellular epithelial component and the surrounding support stroma. Generally, the hallmark of an epithelial malignancy is an increase in the overall epithelial cell density with increased nuclear and nucleolar size. To facilitate invasion into the surrounding stroma, subcellular compositional changes in that matrix structure also occur. Microscopic subcellular alterations exist that may not be apparent in standard pathological analysis. Macroscopic scattering of light from tissue is

Address all correspondence to Brian Pogue, Thayer School of Engineering, Dartmouth College, 8000 Cummings Hall, Hanover, NH 03755. Tel.: (603) 646-3861; Fax: (603) 646-3856; E-mail: pogue@dartmouth.edu

thought to originate from the multiple microscopic fluctuations in refraction index between intracellular organelles and extracellular structures, typically bounded by bilipid membranes.^{21–23} Origin of the transport scattering coefficient, which can be measured tomographically, is likely to result from these differences in the index of refraction between the extracellular or cytoplasmic fractions of tissue and the lipid composition of the membranes bounding each cell and cellular organelle. Hence, variations in the scattering spectral features, which can be measured tomographically, may encode morphologic and pathophysiologic changes in tissue at the microscopic level. While it is possible to postulate causes of scattering in tissue, it is considerably more difficult to design objective experiments that prove a given hypothesis. Several studies have demonstrated that light transport in tissue is dominated by elastic scattering. The applicability of Mie theory is only approximate because it strictly applies only for spheres in a homogenous background,^{24,25} yet such approximations have been used successfully in the interpretation of natural scattering phenomenon, and are explained here as a reasonable first-order approximate.²⁶

Previous studies of particle size determination from scattering spectra have been focused on mucosal diseases or dilute cell suspensions where the scattering by cell nuclei has been a primary emphasis,^{9–13,19,20} and in general an increased nuclear scatterer size has been found in diseased tissue. In these studies, subtle oscillations in the scattering spectrum were used to estimate nuclear size through fits to Mie calculations. In other investigations, more focus has been paid to the scattering of small particles in tissue. However, the extent to which small and large particle size scatterers can be simultaneously fit with sparse data is not yet clear, although with full angular or spectral reflectance, it is evident that reasonable estimation of both can be achieved.^{27–30} Mie scattering interpretation serves as a reasonable starting point to analyze elastic transport scattering spectra, and with sparse wavelength data, it appears likely that only information about smaller scattering particles can be effectively estimated.

In all prior attempts to estimate particle size, some assumptions have been made about the histogram of particle sizes in tissue, which then enables the estimation problem to be reduced to only two parameters, namely, the mean particle size and number density. For larger particles, like cell nuclei, the histogram shape has been assumed to be Gaussian.^{11,28,31–33} However, smaller particles, like mitochondria, golgi bodies, lysosomes, etc., have often been assumed to be arranged in a log-normal distribution.¹⁰ There is also a strong rationale for using a simple exponential function for the distribution of smaller particles in tissue, as the density of smaller organelle structures clearly continues to decrease well below our ability to image these structures with optical microscopy. In tissue phantom studies, Intralipid provides a distribution of sizes where the histogram has been determined by electron microscopy to be exponentially distributed²⁴ with a mean particle size of 97 nm. In this paper, we use the exponential distribution of particle sizes to interpret the scattering spectra of both Intralipid and human breast tissue.

One of the goals of NIR tomography research has been to provide clinicians with new information about the underlying properties of benign and malignant breast disease.^{7,34–37} However, there is emerging data indicating that NIR scattering

spectra are correlated to the normal composition of breast tissue, and that changes in breast physiology can be detected by variations in scattering spectra.^{38,39} In mammography, there are four classifications of breast density that are designated in the BI-RADS (American College of Radiology Breast Imaging Reporting and Data System) lexicon:⁴⁰ almost entirely fat (fatty), scattered fibroglandular (scattered), heterogeneously dense (HD), and extremely dense (ED). In this study, these classifications are used as a basis for categorizing normal breast tissues into groups, where prior results have indicated a good correlation between scattering and the increase in radiographic density category when a group of women with mammographically normal breast were imaged.⁴¹

In this paper, a method for extracting the mean particle size and number density from the reduced scattering coefficient spectrum is proposed. The scattering spectrum was sampled at six wavelengths (661, 761, 785, 808, 826, and 849 nm) measured for transmission through normal breast tissue using a clinical breast tomography system. The assumptions and limitations of the fitting process are discussed to put the study in perspective with prior work, and the method utilized is analyzed through simulated and tissue-phantom data to establish its accuracy. The value of estimating particle size and number density from tomography data could be quite significant; hence, methods to further test and implement the approach are discussed.

2 Methods

2.1 Mie Theory Interpretation

Mie theory provides an exact solution for the scattering and the anisotropy coefficients of perfect dielectric spheres of arbitrary size in a uniform background medium.^{24,25} Using this theoretical framework, the reduced scattering spectra of bulk homogeneous samples can be approximately expressed by the following equation:

$$\mu'_s(\lambda) = N_o(\pi a^2) Q_{\text{scat}}(m, a, \lambda) [1 - g(m, a, \lambda)], \quad (1)$$

where λ is the wavelength, a is the particle size (the diameter of the particle), m is the refractive index ratio from inside to outside the particles ($m = n_2/n_1$, where n_1 and n_2 are the refractive index outside and inside the particles, respectively), and $Q_{\text{scat}}(m, a, \lambda)$ is a dimensionless scattering efficiency factor that is calculated from an analytic series expansion, which is the solution to the scattered wave intensity from the sphere.²⁵ This expression is used to estimate the refraction and reflection from a spherical particle. The framework can be extended to approximate a multisized scattering particle medium by summing the scattering contributions over all particle sizes and adding an approximate normalized size distribution factor $f(a)$ that compensates for the number of particles at each given size, in which case Eq. (1) becomes

$$\mu'_s(\lambda) = N_o \sum_{i=1}^p f(a_i) (\pi a_i^2) Q_{\text{scat}}(m, a_i, \lambda) [1 - g(m, a_i, \lambda)]. \quad (2)$$

This equation has implicit assumptions that the particle index changes are all the same, which is a limitation that should be

recalled when it is applied in various problems. However, it is possible that index changes typically result only in changes of amplitude in μ'_s , rather than changes in the spectral features in the NIR regime. Thus, while the assumption of constant n is unfortunate, it still does enable an estimation of the particle size, given some *a priori* information about the $f(a_i)$ function, which describes the histogram of particle number density per unit particle size.

Since the reduced scattering spectra $\mu'_s(\lambda)$ depends on the histogram of particle number density per unit particle size $f(a_i)$, it is important to carefully analyze how these particular functions might impact the results of the study. Three histogram shapes have been examined, including (1) a step function, (2) a normalized Gaussian function, and (3) an exponentially decaying function. Each is used with the same average particle size and the same total number density to determine differences in μ'_s caused by different histogram shape assumptions.

In Eq. (2), the particle number density only changes the magnitude of the scattering coefficients, but not the shape of the scattering spectra. Thus we are only required to consider the three parameters: (1) histogram shape, (2) average particle size, and (3) refractive index ratio m when evaluating the shape of the scattering spectra. By setting two of the parameters to be the same, we can observe the influence of the third parameter on the scattering spectra.

2.2 Scattering Spectra Power Law Fit

Rather than applying Mie scattering theory directly, a more empirical approach was first proposed by van Staveren et al.,²⁴ who fit the scattering spectrum of Intralipid. A number of groups have adopted the approach to characterize the spectrum of the reduced scattering coefficient observed in tissues.^{36,39,42,43} In these studies, the scattering spectra are considered to satisfy a power law relationship. Empirically, when there is a broad range of scattering particle sizes, this spectrum is described by a power law curve of the type:

$$\mu'_s(\lambda) = A\lambda^{-b}, \quad (3)$$

where A and b are model parameters for scattering amplitude and scattering power, respectively. Equation (3) describes a smooth function with no oscillations in the spectrum, and conveniently restricts the fitting process to only two parameters. The curve is quasilinear in the NIR region, and appears to fit data from a large number of wavelengths reasonably well.⁴⁴

2.3 Scattering from Tissue Spectra

Reduced scattering coefficients at 6 wavelengths have been obtained with an experimental clinical imaging system (described in detail elsewhere.⁴⁵) The limited number of wavelengths is not sufficient for identifying oscillations in the scattering spectra of the type that might be observed from larger Mie scattering particles, as observed in Fig. 1(d) in Sec. 3 for the 10 μm sized particles. Nonetheless, if it is assumed that the dominant particle sizes are smaller and thus the large particle oscillations are small, the data may be used to compare with Mie theory calculations in the wavelength range 660 to 850 nm. To estimate particle size and number density, the six experimental reduced scattering coefficients are fit to

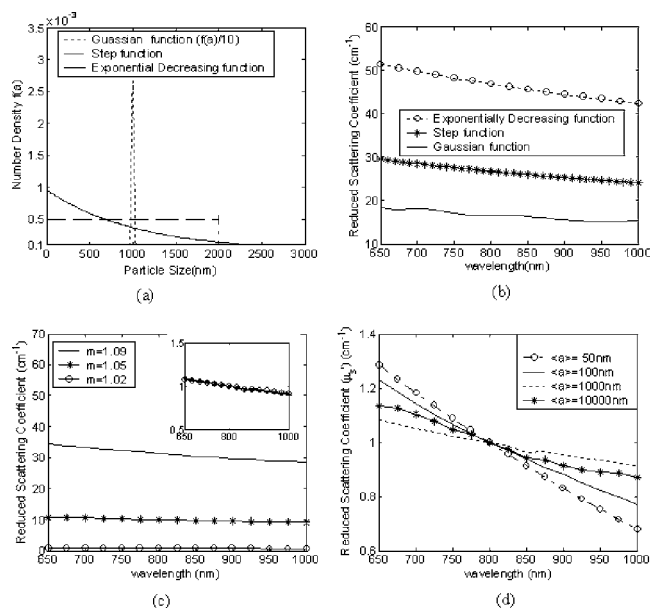


Fig. 1 (a) Comparison of Gaussian, uniform, and exponential particle size distributions with the same average particle size $\langle a \rangle = 1000$ nm; (b) calculated reduced scattering spectra for these three particle size distributions with the same refractive index change ($n_1 = 1.311$ and $n_2 = 1.451$); (c) comparison of reduced scattering spectra for three different refractive indexes for the same size distribution with average particle size $\langle a \rangle = 1000$ nm, where the inset plot is the comparison of these three spectra after being normalized at 800 nm; and (d) comparison of reduced scattering spectra for four different average particle sizes with the same exponential size distribution and refractive index ($n_1 = 1.36$, $n_2 = 1.4$).

predictions of the power law expression in Eq. (3), first to get the scattering amplitude and scattering power, and then to generate the reduced scattering coefficients at 15 wavelengths (650, 675, 700, 725, 750, 775, 800, 825, 850, 875, 900, 925, 950, 975, and 1000 nm). For extracting the average particle size, we normalize these 15 reduced scattering coefficients at one wavelength (we selected 800 nm). By normalizing the scattering coefficients, we eliminate the influence of number density, so only one parameter (average particle size) is required in the first fitting. Comparing these 15 data with Mie theory results from Eq. (2) (also normalized at 800 nm) using a least-squares minimization, the average particle size can be effectively estimated. With the average particle size established, the number density can then be estimated by comparing the original 15 data (no normalization) with Mie theory [Eq. (2)] using a second least-squares minimization method. In the least-squares minimization method, the deviation of the experimental data from the Mie prediction is expressed as the error function:

$$\chi = \left\{ \frac{1}{n} \sum_{i=1}^n [(\mu_s^{i_{\text{exp}}} - \mu_s^{i_{\text{theo}}}) / \mu_s^{i_{\text{theo}}}]^2 \right\}^{1/2} \quad (4)$$

where χ is the error norm, calculated as the least-squares difference between the experimental data and the Mie theory. Here, n is the total number of wavelengths at which we have the reduced scattering coefficient data, $\mu_s^{i_{\text{exp}}}$ is the experimental reduced scattering coefficient at the i 'th wavelength,

$\mu_s^{i_0}$ is the reduced scattering coefficient at the i 'th wavelength calculated from Mie theory. In this study, no attempt was made to perform a nonlinear fit, but rather all possible values of mean size and mean density were calculated, and the minimum value of χ was used to determine the best estimate.

2.4 Simulation Study

Intralipid is a fat emulsion that is used clinically as an intravenously administered nutrient and provides a convenient scattering component in a tissue phantom to investigate propagation of light in tissue.²⁴ For Intralipid, there is considerable evidence to suggest its particle distribution is exponential, especially considering the dominant fraction of Rayleigh scattered light that occurs in the blue region of the spectrum.⁴⁶ In the van Stanveren et al. paper,²⁴ the size distribution of the scattering particles in 10% Intralipid was determined by transmission electron microscopy to be exponential and the average particle size was reported to be 97 ± 3 nm. If the functional form of $f(a_i)$ is a normalized exponential function with respect to a_i ,

$$f(a_i) = \frac{\exp(-a_i/\langle a \rangle)}{\langle a \rangle}, \quad (5)$$

then the average particle size $\langle a \rangle$ can be estimated by an iterative fit between the data and this model.

To validate the method, simulated data were used to test the fitting process. The mean particle size in the simulation study was selected in the smaller size range (< 1000 nm), which is the size range of collagen fiber networks in the extracellular matrix, mitochondria, and other intracellular vesicles,⁴⁷ but do not include the larger size, such as that of cell nuclei, typically 5 to 15 μm in diameter. The first five groups of simulated data included the following mean size and mean number densities: (1) $\langle a \rangle = 50$ nm, $N = 1 \times 10^{19} \text{ m}^{-3}$; (2) $\langle a \rangle = 100$ nm, $N = 1 \times 10^{19} \text{ m}^{-3}$; (3) $\langle a \rangle = 200$ nm, $N = 1 \times 10^{19} \text{ m}^{-3}$; (4) $\langle a \rangle = 500$ nm, $N = 1 \times 10^{19} \text{ m}^{-3}$; and, (5) $\langle a \rangle = 1000$ nm, $N = 1 \times 10^{19} \text{ m}^{-3}$. These data were generated computationally using the expression in Eq. (2) for the six wavelengths that are available in our tomography system. These data were used as synthetic scattering spectra to determine how accurately the fitting process can be completed.

2.5 Phantom Studies

The tomography system was used to validate the particle size fitting approach with data from tissue-simulating phantoms. Liquid phantoms were used, composed of Intralipid at 11 different concentrations, to obtain a reduced scattering coefficient spectrum at six wavelengths. The data at each concentration was analyzed with the method already described for estimating the average particle size and number density. By varying the concentration, each spectrum should result in the same particle size (97 ± 3 nm, according to the van Staveren et al. paper²⁴) as only the number density in the liquid is altered when the concentration varies. Thus, the ratio of number density over concentration should be constant for these test solutions.

2.6 Clinical Studies

In a final step, the fitting method was applied to normal breast tissue data. The study was approved by the institutional committee for the protection of human subjects. NIR imaging studies were performed on asymptomatic women recruited into the study following a negative mammogram. Informed consent was provided prior to the NIR imaging exam. Normal subjects were stratified by age (i.e., 10-y intervals) and by one of four radiographic density categories (fatty, scattered, HD, and ED). Data from 31 normal subjects were used; right and left breasts were analyzed separately. Scattering coefficient spectra at the six wavelengths were estimated for the entire slice tissue, and these were fit with the algorithm. Average particle size and number density were determined from the spectra, and the resulting data were grouped according to the radiographic density of the subjects.

3 Results

3.1 Influence of Particle Size Distribution

The influence of parameter selections on the resulting reduced scattering spectra is shown for a specific case in Fig. 1, where the effects of (1) size distribution function, (2) average particle size, and (3) index of refraction change are illustrated. Figure 1(a) indicates the relative shape of the three distribution functions (i.e., histogram shapes) considered, a Gaussian function, $f(a) = \exp[-(a-1000)^2/2 \times 10^2]/25$; a step function [if $0 < a < 2000$, $f(a) = 1/2000$; otherwise, $f(a) = 0$]; and an exponential decreasing function [$f(a) = 9.5 \times 10^{-4} \times \exp(-9.5 \times 10^{-4}a)$]. They are normalized and have the same average particle size ($\langle a \rangle = 1000$ nm). For the Gaussian distribution with a small variance, most particles are clustered around 1000 nm. For the step function, the particles are distributed evenly between zero and 2000 nm, for the exponential function, more particles exist in the smaller size range. A comparison of scattering spectra among these three different histogram shapes with the same average particle size and same refractive index $n_1 = 1.311$, $n_2 = 1.451$, is shown in Fig. 1(b). In this graph, the exponential distribution has the largest scattering coefficient, while the Gaussian distribution has the smallest one. Based on this result and the distribution characteristics of these three functions, it is evident that particles with smaller sizes have more impact on the magnitude of the scattering spectrum in the wavelength range 650 to 1000 nm. This figure also shows the characteristic oscillatory components in the scattering spectrum associated with the Gaussian distribution that were observed in other epithelial studies of elastic scattering.

The comparison of reduced scattering coefficients among three different sets of refractive indices is shown in Fig. 1(c). These results were calculated with the same exponential size distribution, and average particle size, but with refractive index values of $n_1 = 1.33$, $n_2 = 1.45$ ($m = 1.09$); $n_1 = 1.33$, $n_2 = 1.40$ ($m = 1.05$); and the smallest set $n_1 = 1.33$, $n_2 = 1.35$ ($m = 1.02$). The figure indicates that as the difference between two refractive indices increases, the scattering intensity increases. The scattering spectra were also normalized at 800 nm [inset graph in Fig. 1(c)] to observe whether differences in spectral shape are caused by changes in relative refractive index $m = n_2/n_1$. It is clear that in the spectral shape

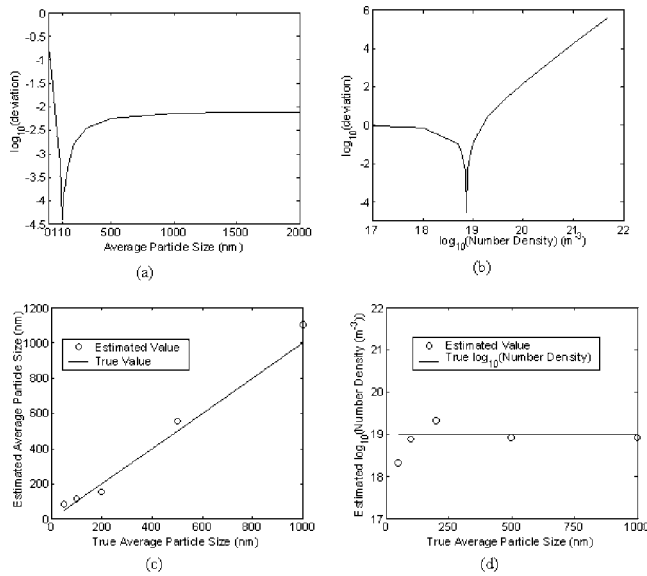


Fig. 2 (a) Error function for estimating average particle size using simulated test data with a true average particle size of $\langle a \rangle = 100$ nm. The minimum of the function presents the optimal estimation of particle size. (b) The same for number density assuming an average particle size $\langle a \rangle = 100$ nm and number density $N = 1 \times 10^{19} \text{ m}^{-3}$. (c) Estimates of average particle size based on test data with true values of $\langle a \rangle = 50, 100, 200, 500,$ and 1000 nm, with $N = 1 \times 10^{19} \text{ m}^{-3}$ and (d) corresponding estimates of number density, indicating that number density does not change significantly with changes in particle size.

changes are nominal; hence, the assumption in Eq. (2) that refractive indices are the same for all particle sizes appears reasonable.

The reduced scattering coefficients obtained from four different average particle sizes, $\langle a \rangle = 50, 100, 1000,$ and $10,000$ nm for the exponential particle size distribution and same refractive indices ($n_1 = 1.36, n_2 = 1.40$) are presented in Fig. 1(d). The scattering spectra were normalized at 800 nm to investigate potential shape changes caused by the average particle size. Here, increasing the average particle size in the range of 50 to 1000 nm generates a reduced scattering coefficient spectrum that has a smaller overall slope but more oscillatory components. This result is consistent with the prior findings of Mourant et al.⁴³ By normalizing the scattering spectra at one wavelength and then comparing it to Mie theory, we are able to extract the average particle size by least-squares minimization.⁴⁸

3.2 Simulation Results of the Optimal Estimated Values for Particle Size and Number Density

The least-squares minimization method described in Eq. (5) was used to estimate the optimal values for particle size and number density. For simulated test data with a true average particle size of $\langle a \rangle = 100$ nm and $N = 1 \times 10^{19} \text{ m}^{-3}$, the estimated particle size and number density were 110 nm and $0.75 \times 10^{19} \text{ m}^{-3}$. These results are shown in Fig. 2, which indicates that a unique fitted solution is available through the optimization process. The estimates of average particle size for simulated data with true values of average particle sizes of $\langle a \rangle = 50, 100, 200, 500,$ and 1000 nm, and number densities of $N = 1 \times 10^{19} \text{ m}^{-3}$, were 80, 110, 150, 550, and 1100 nm,

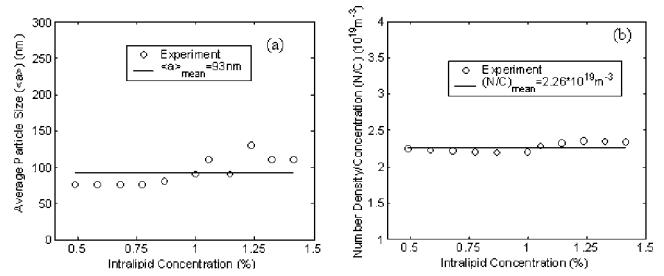


Fig. 3 Estimates of average particle size for Intralipid phantoms with varying (a) concentration and (b) number Density.

respectively, for average size and $2 \times 10^{18}, 7.5 \times 10^{18}, 2 \times 10^{19}, 8 \times 10^{18},$ and $8 \times 10^{18} \text{ m}^{-3}$, respectively, for number density. The results are also shown in graphical form in Fig. 2 and indicate that the extraction method is reasonably robust and accurate when fitting simulated data.

3.3 Estimated Values of Particle Size and Number Density of Intralipid Phantoms

Estimates of average particle size and number density were obtained for 11 different concentrations of Intralipid, and are presented in Fig. 3. The average particle size results ranged from 75 to 130 nm. Over the 11 concentrations used here, the mean average particle size was 93 nm, with a standard deviation of 19 nm. This value is close to the Intralipid particle size estimated from electron microscopy reported (97 ± 3 nm) in the paper by van Staveren et al.²⁴ The estimated number density ranged from 1.1×10^{19} to $3.3 \times 10^{19} \text{ m}^{-3}$, which when divided by Intralipid concentration spanned 2.19×10^{19} to $2.35 \times 10^{19} \text{ m}^{-3}$. Overall these 11 concentrations, the mean value of number density divided by concentration was $2.26 \times 10^{19} \text{ m}^{-3}$, with standard deviation $0.06 \times 10^{19} \text{ m}^{-3}$. The ratio of the number density over concentration is essentially constant for the 11 concentrations as expected. In addition, it appears that Fig. 3(a) includes a systematic underestimation of the size below 1% Intralipid, and an overestimation above.

3.4 Estimated Values of Particle Size and Number Density of Normal Subjects with Different Radiographic Density Categories

Normal breast tissue types of normal breasts were grouped into one of four radiographic density categories (fatty, scattered, HD, ED). A clear difference in the mean average particle size and number density for these four compositions of breast tissue was found and shown in Fig. 4. For the ED breast type, the average particle size ranged from 20 to 65 nm, with a mean of 36 ± 16 nm. For the HD breast type, the average particle sizes spanned 25 to 200 nm, with a mean of 68 ± 40 nm. For the scattered type breast, the average particle sizes covered 140 to 1200 nm, with a mean of 318 ± 330 nm. Finally, for the fatty type breast, average particle sizes from 150 to 1400 nm were found, with a mean of 485 ± 461 nm. The composite data are summarized in Table 1. Over the sequence of increasing mean particle size with breast tissue type (ED, HD, scattered, and fatty), there is a concordant decrease of the number density.

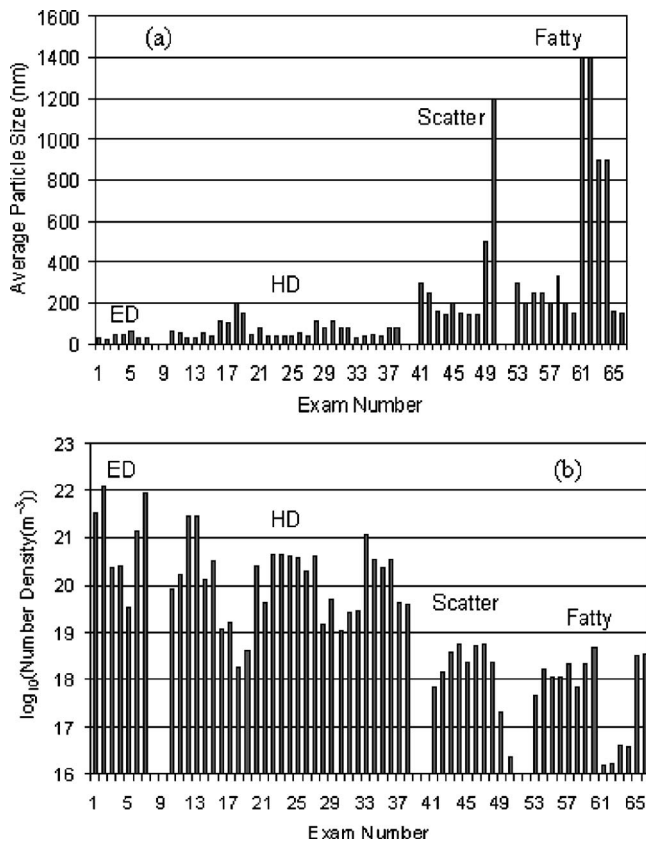


Fig. 4 Average particle sizes from individual normal subject exams grouped by (a) radiographic density and (b) number density.

4 Discussion

Overall, the results indicate that by defining the particle size distribution function, and assuming values of refractive index ratio, based on the water-to-lipid membrane change, Mie theory can be used to estimate an effective mean particle size and number density of breast tissue. The estimates were derived from bulk transport scattering measurements at six discrete wavelengths, 661, 761, 785, 808, 826, and 849 nm, assuming that the reduced scattering spectrum is smooth in shape across the wavelength range. As shown in Fig. 1, smaller particle sizes lead to similar reduced transport scattering spectra with little oscillation, whereas particles above

1 μm in mean size generate visible oscillations in the reduced scattering spectra as a function of wavelength. Thus, any smoothness assumption in scattering spectrum inherently limits the results to estimating smaller average particle sizes. The scattering spectra currently reported for bulk breast tissue do not show significant presence of oscillations as a function of wavelength.^{5,42,44,49} While this observation could be an artifact of the data processing, it is also reasonable to assume that the dominant scattering particle sizes are less than 1 μm . Although larger structures, such as cell nuclei, typically 5 to 15 μm in diameter, are known to scatter light, it is certainly true that the largest number of membrane bound structures in tissue are considerably smaller than the nucleus. When imaging cells with phase contrast microscopy, the total backscatter due to the cytoplasm is typically much more significant than the nucleus, indicating that intracellular structures other than the nucleus are important determinants of the scattering spectra. The primary small scattering centers in tissue are thought to be the collagen fiber network of the extracellular matrix, the mitochondria, and other intracellular entities with dimensions smaller than the optical wavelengths.⁴⁷ Nonetheless, this assumption is an unsatisfactory compromise, but one that is routinely employed in elastic scattering spectroscopy, and should be further studied. Yet given the difficulties in extracting subwavelength information from samples, it is likely a problem without an easy solution at this point in time.

Given these assumptions and limitations, a fitting procedure is possible where the normalized scattering spectra are used to estimate mean particle size first, and then number density can be readily determined. In making assumptions about the exponential shape of the histogram of particle sizes, and in restricting the data to a sparse number of wavelengths, there is inherent neglect of any oscillatory spectral components that may be present. A third assumption in the procedure used $m=1.09$, as the refractive index ratio between intra- and extracellular cytoplasm and fluid and the bilipid membrane. As seen in Fig. 1(c), changes in this parameter appear to affect only the overall magnitude of the scattering spectra, without altering its slope. Thus, even if this parameter were in error, it appears likely that it would lead to an error in number density rather than mean particle size. Figure 1 suggests that the strongest effect on the scattering spectra shape was mean particle size; thus, even given the significant assumptions in-

Table 1 Average particle size and number density estimated from mean scattering spectrum data acquired *in vivo* from normal breasts, where the scattering coefficients were taken as the whole breast average obtained for each subject.

Breast Type (n =Number of Subjects)	Mean Size (nm) \pm SD	Size Range (nm) Min-Max	$\log_{10}[N(/m^3)] \pm$ SD	$\log_{10}[N(/m^3)]$ Range Min-Max
ED ($n=4$)	36 ± 16	20–65	21.00 ± 0.94	19.52–22.08
HD ($n=15$)	68 ± 40	25–200	20.03 ± 0.79	18.28–21.45
S ($n=5$)	318 ± 330	140–1200	18.12 ± 0.77	16.36–18.76
F ($n=7$)	485 ± 461	150–1400	17.71 ± 0.90	16.20–18.68

ED=extremely dense; HD=heterogeneously dense; S=scattered fibroglandular densities; F=Almost entirely fat

voked here, that the fitting process is expected to be reasonably accurate in bulk tissue spectroscopy. Estimating Intralipid solutions in this manner worked quite well, and the extension to bulk tissue data appears reasonably good. Hence, the absolute values for mean particle size are likely more reliable than their number density counterparts. Nonetheless, relative changes in both parameters are likely to be quite reliable between samples and between tissue types.

The results show that there are significant changes in the mean particle size and the number density estimation from tomographic imaging between different breast tissue types. Taking into account the limited number of normal volunteers examined, the grouping of the data in terms of the four density classifications is not as well defined as our previous study of scattering power and amplitude,^{39,50} but the overall trend agrees with what would be expected physiologically. This analysis was applied retrospectively to normal whole breast spectra accumulated in our ongoing clinical exam accruals to examine how particle size and number density vary with physiological differences.^{39,50} Mean particle sizes of 20 to 1400 nm were observed, which are consistent with sub-cellular organelles and collagen matrix fibrils. Further study of this type of analysis could lead toward a better understanding of how microscopic variations could be detected from bulk tissue measurements, and potentially how these may vary with pathological change.

There are several potential ways to improve the accuracy and precision of the mean particle size estimates reported here. The accuracy is likely to be increased by increasing the number of wavelengths (15 instead of 6) used to recover the reduced scattering coefficient spectrum and/or their wider distribution in the spectrum. Simulation results indicate that the fitting algorithm improves with increased number of wavelengths; however, our current tomography system is limited to 6 wavelengths, although more could be added in the future. Another approach to improving the estimate is to measure the particle size histogram specifically, as was done explicitly for Intralipid in the paper by van Staveren et al.²⁴ This may be challenging because it is not evident that electron microscopy shows the same contrast as optical scattering, so the relation between the two may not be direct; however, other approaches such as studying the angular scattering dependence of thin samples may lead to similar information.^{9,12} The method provided in this paper provides a good estimation for mean particle size and number density for the exponentially distributed particles in smaller size range. While work in these areas is ongoing, the current study indicates that scattering particle size varies with radiographic density, as might be expected from the variety of tissue constituents within these different compositional types of breast tissue, and that Mie theory can be used as a first-order approximation of these parameters.

Acknowledgments

This research was supported by grants PO1CA80139 and U54CA105480. The authors are very grateful to Adam Wax, PhD (Duke University), for useful discussions about how to approach the problem of fitting particle size and density sequentially from a scattering coefficient data set.

References

1. B. J. Tromberg, N. Shah, R. Lanning, A. Cerussi, J. Espinoza, T. Pham, L. Svaasand, and J. Butler, "Non-invasive *in vivo* characterization of breast tumors using photon migration spectroscopy," *Neoplasia* **2**(1-2), 26-40 (2000).
2. A. E. Cerussi, D. Jakubowski, N. Shah, F. Bevilacqua, R. Lanning, A. J. Berger, D. Hsiang, J. Butler, R. F. Holcombe, and B. J. Tromberg, "Spectroscopy enhances the information content of optical mammography," *J. Biomed. Opt.* **7**(1), 60-71 (2002).
3. B. W. Pogue, T. O. McBride, C. Nwaigwe, U. L. Osterberg, J. F. Dunn, and K. D. Paulsen, "Near-infrared diffuse tomography with *a priori* MRI structural information: testing a hybrid image reconstruction methodology with functional imaging of the rat cranium," *Proc. SPIE* **3597**, 484-492 (1999).
4. R. Srinivasan and M. Singh, "Laser backscattering and transillumination imaging of human tissues and their equivalent phantoms," *IEEE Trans. Biomed. Eng.* **50**(6), 724-730 (2003).
5. R. Cubeddu, C. D'Andrea, A. Pifferi, P. Taroni, A. Torricelli, and G. Valentini, "Effects of the menstrual cycle on the red and near-infrared optical properties of the human breast," *Photochem. Photobiol.* **72**(3), 383-391 (2000).
6. S. Fantini, M. A. Franceschini, G. Gaida, E. Gratton, H. Jess, W. W. Mantulin, K. T. Moesta, P. M. Schlag, and M. Kaschke, "Frequency-domain optical mammography: edge effect corrections," *Med. Phys.* **23**, 149-157 (1996).
7. V. Ntziachristos, A. G. Yodh, M. D. Schnall, and B. Chance, "MRI-guided diffuse optical spectroscopy of malignant and benign breast lesions," *Neoplasia* **4**(4), 347-354 (2002).
8. B. W. J. Pogue, X. Song, S. Srinivasan, H. Dehghani, K. D. Paulsen, T. D. Tosteson, C. Kogel, S. Soho, and S. Poplack, "Near-Infrared scattering spectrum differences between benign and malignant breast tumors measured *in vivo* with diffuse tomography," in *OSA Biomedical Optics Topical Meetings, Technical Digest*, p. ThB1 (2004).
9. J. R. Mourant, T. M. Johnson, and J. P. Freyer, "Characterizing mammalian cells and cell phantoms by polarized backscattering fiberoptic measurements," *Appl. Opt.* **40**(28), 5114-5123 (2001).
10. V. Backman, V. Gopal, M. Kalashnikov, K. Badizadegan, R. Gurjar, A. Wax, I. Georgakoudi, M. Mueller, C. W. Boone, R. R. Dasari, and M. S. Feld, "Measuring cellular structure at submicrometer scale with light scattering spectroscopy," *IEEE J. Sel. Top. Quantum Electron.* **7**(6), 887-893 (2001).
11. L. T. Perelman, V. Backman, M. Wallace, G. Zonios, R. Manoharan, A. Nusrat, S. Shields, M. Seiler, C. Lima, T. Hamano, I. Itzkan, J. Van Dam, J. M. Crawford, and M. S. Feld, "Observation of periodic fine structure in reflectance from biological tissue: a new technique for measuring nuclear size distribution," *Phys. Rev. Lett.* **80**(3), 627 (1998).
12. A. Wax, C. Yang, V. Backman, M. Kalashnikov, R. R. Dasari, and M. S. Feld, "Determination of particle size by using the angular distribution of backscattered light as measured with low-coherence interferometry," *J. Opt. Soc. Am. A* **19**(4), 737-744 (2002).
13. A. Wax, C. Yang, V. Backman, K. Badizadegan, C. W. Boone, R. R. Dasari, and M. S. Feld, "Cellular organization and substructure measured using angle-resolved low-coherence interferometry," *Biophys. J.* **82**, 2256-2264 (2002).
14. R. Graaff, J. G. Aarnoudse, J.-R. Zijp, P.-M. A. Sloot, F. F. M. de Mull, J. Greve, and M. H. Koelink, "Reduced light-scattering properties for mixtures of spherical particles: a simple approximation derived from Mie calculations," *Appl. Opt.* **31**(10), 1370-1376 (1992).
15. A. M. K. Nilsson, C. Sturesson, D. L. Liu, and S. Andersson-Engels, "Changes in spectral shape of tissue optical properties in conjunction with laser-induced thermotherapy," *Appl. Opt.* **37**(7), 1256-1272 (1998).
16. B. T. E. Gelebart, J. M. Tualle, and S. Avriillier, "Phase function simulation in tissue phantoms: a fractal approach," *Pure Appl. Opt.* **5**(4), 377-388 (1996).
17. J. M. Schmitt and G. Kumar, "Optical scattering properties of soft tissue: a discrete particle model," *Appl. Opt.* **37**(13), 2788-2797 (1998).
18. R. K. Wang, "Modelling optical properties of soft tissue by fractal distribution of scatterers," *J. Mod. Opt.* **47**(1), 103-120 (2000).
19. H. K. Roy, Y. Liu, R. K. Wali, Y. L. Kim, A. K. Kromine, M. J. Goldberg, and V. Backman, "Four-dimensional elastic light-scattering fingerprints as preneoplastic markers in the rat model of colon carcinogenesis," *Gastroenterology* **126**(4), 1071-1081 (2004).

20. I. J. Bigio, S. G. Bown, G. Briggs, C. Kelley, S. Lakhani, D. Pickard, P. M. Ripley, I. G. Rose, and C. Saunders, "Diagnosis of breast cancer using elastic-scattering spectroscopy: preliminary clinical results," *J. Biomed. Opt.* **5**(2), 221–228 (2000).
21. R. Drezek, A. Dunn, and R. Richards-Kortum, "Light scattering from cells: finite-difference time-domain simulations and goniometric measurements," *Appl. Opt.* **38**(16), 3651 (1999).
22. H. B. Liu, M. Kimura, and B. Chance, "Dependence of tissue optical properties on solute-induced changes in refractive index and osmolarity," *J. Biomed. Opt.* **1**, 200–211 (1996).
23. B. Chance, Q. Luo, S. Nioka, D. C. Alsop, and J. A. Detre, "Optical investigations of physiology: a study of intrinsic and extrinsic biomedical contrast," *Philos. Trans. R. Soc. London, Ser. B* **352**, 707–716 (1997).
24. H. J. van Staveren, C. J. M. Moes, J. van Marle, S. A. Prahl, and M. J. C. van Gemert, "Light scattering in intralipid-10% in the wavelength range of 400–1100 nm," *Appl. Opt.* **30**(31), 4507–4514 (1991).
25. C. F. Bohren and D. R. Huffman, *Absorption and Scattering of Light by Small Particles*, Wiley, New York (1998).
26. H. C. van de Hulst, *Light Scattering by Small Particles*, Dover, New York (1981).
27. V. Backman, R. S. Gurjar, L. T. Perelman, V. Gopal et al., "Imaging and measurement of cell structure and organization with submicron accuracy using light scattering spectroscopy," in *Optical Biopsy IV*, *Proc. SPIE* **4613**, 101–110 (2002).
28. J. R. Mourant, J. P. Freyer, A. H. Hielscher, A. A. Eick, D. Shen, and T. M. Johnson, "Mechanisms of light scattering from biological cells relevant to noninvasive optical-tissue diagnostics," *Appl. Opt.* **37**(16), 3586–3593 (1998).
29. H. Jiang, "Subcellular sizing with polarized light spectroscopy," *Opt. Commun.* **226**(1–6), 279–283 (2003).
30. A. H. Hielscher, J. R. Mourant, and I. J. Bigio, "Influence of particle size and concentration on the diffuse backscattering of polarized light from tissue phantoms and biological cell suspensions," *Appl. Opt.* **36**(1), 125–135 (1997).
31. A. Wax, C. H. Yang, M. G. Muller, R. Nines, C. W. Boone, V. E. Steele, G. D. Stoner, R. R. Dasari, and M. S. Feld, "In situ detection of neoplastic transformation and chemopreventive effects in rat esophagus epithelium using angle-resolved low-coherence interferometry," *Cancer Res.* **63**, 3556–3559 (2003).
32. H. B. Jiang, "Frequency-domain fluorescent diffusion tomography: a finite-element-based algorithm and simulations," *Appl. Opt.* **37**(22), 5337–5343 (1998).
33. H. Jiang, G. Marquez, and L. V. Wang, "Determination of particle size distribution in concentrated suspensions: photon migration approach," in *OSA Trends Opt. Photonics Ser.* **21**, 92 (1998).
34. B. J. Tromberg, O. Coquoz, J. B. Fishkin, T. Pham, E. R. Anderson, J. Butler, M. Cahn, J. D. Gross, V. Venugopalan, and D. Pham, "Non-invasive measurements of breast tissue optical properties using frequency-domain photon migration," *Philos. Trans. R. Soc. London, Ser. B* **352**, 661–668 (1997).
35. T. Durduran, R. Choe, J. P. Culver, L. Zubkov, M. J. Holbroke, J. Giammarco, B. Chance, and A. G. Yodh, "Bulk optical properties of healthy female breast tissue," *Phys. Med. Biol.* **47**(16), 2847–2861 (2002).
36. B. W. Pogue, S. P. Poplack, T. O. McBride, W. A. Wells, O. K. S., U. L. Osterberg, and K. D. Paulsen, "Quantitative hemoglobin tomography with diffuse near-infrared spectroscopy: pilot results in the breast," *Radiology* **218**(1), 261–266 (2001).
37. S. P. Poplack, K. D. Paulsen, A. Hartov, P. M. Meaney, B. W. Pogue, T. C. Tosteson, M. R. Grove, S. K. Soho, and W. A. Wells, "Electromagnetic breast imaging: average tissue property values in women with negative clinical findings," *Radiology* **231**, 571–580 (2004).
38. K. Blyschak, M. K. Simick, R. A. Jong, and L. D. Lilje, "Classification of breast tissue density by optical transillumination spectroscopy: optical and physiological effects governing predictive value," *Proc. SPIE* **5260**, 568–579 (2003).
39. S. Srinivasan, B. W. Pogue, S. Jiang, H. Dehghani, C. Kogel, S. Soho, J. G. Chambers, T. D. Tosteson, S. P. Poplack, and K. D. Paulsen, "Interpreting hemoglobin and water concentration, oxygen saturation, and scattering measured by near-infrared tomography of normal breast in vivo," *Proc. Natl. Acad. Sci. U.S.A.* **100**(21), 12349–12354 (2003).
40. E. Ziv, J. Shepherd, R. Smith-Bindman, and K. Kerlikowske, "Mammographic breast density and family history of breast cancer," *J. Natl. Cancer Inst.* **95**(7), 556–558 (2003).
41. B. W. Pogue, S. Jiang, H. Dehghani, C. Kogel, S. K. Soho, X. Song, S. Srinivasan, T. D. Tosteson, S. P. Poplack, and K. D. Paulsen, "Characterization of hemoglobin, water and NIR scattering in breast tissue: analysis of inter-subject variability and menstrual cycle changes," *J. Biomed. Opt.* **9**(3), 541–552 (2004).
42. A. E. Cerussi, A. J. Berger, F. Bevilacqua, N. Shah, D. Jakubowski, J. Butler, R. F. Holcombe, and B. J. Tromberg, "Sources of absorption and scattering contrast for near-infrared optical mammography [comment]," *Acad. Radiol.* **8**(3), 211–218 (2001).
43. J. R. Mourant, T. Fuselier, J. Boyer, T. M. Johnson, and I. J. Bigio, "Predictions and measurements of scattering and absorption over broad wavelength ranges in tissue phantoms," *Appl. Opt.* **36**(4), 949–957 (1997).
44. F. Bevilacqua, A. J. Berger, A. E. Cerussi, D. Jakubowski, and B. J. Tromberg, "Broadband absorption spectroscopy in turbid media by combined frequency-domain and steady-state methods," *Appl. Opt.* **39**(34), 6498–6510 (2000).
45. S. Jiang, B. W. Pogue, T. O. McBride, M. M. Doyley, S. P. Poplack, and K. D. Paulsen, "Near-infrared breast tomography calibration with optoelastic tissue simulating phantoms," *J. Electron. Imaging* **12**(4), 613–620 (2003).
46. I. S. Saidi, S. L. Jacques, and F. K. Tittel, "Mie and Rayleigh modeling of visible light scattering in neonatal skin," *Appl. Opt.* **34**(31), 7410–7418 (1995).
47. B. Beauvoit, H. Liu, K. Kang, P. D. Kaplan, M. Miwa, and B. Chance, "Characterization of absorption and scattering properties for various yeast strains by time-resolved spectroscopy," *Cell Biophys.* **23**(1–3), 91–109 (1993).
48. J. W. G. Pyhtila, N. Robert, and A. Wax, "Determining nuclear morphology using an improved angle-resolved low coherence interferometry system," *Opt. Express* **11**(25), 3473–3484 (2003).
49. A. B. Amelink, P. L. Martin, S. A. Burgers, and H. J. C. M. Sterenberg, "Single-scattering spectroscopy for the endoscopic analysis of particle size in superficial layers of turbid media," *Appl. Opt.* **42**(19), 4095–4101 (2003).
50. S. P. Poplack, A. N. Tosteson, M. R. Grove, W. A. Wells, and P. A. Carney, "Mammography in 53,803 women from the New Hampshire mammography network," *Radiology* **217**(3), 832–840 (2000).